

## Numerical modelling of time-dependent skin degradation of an isolated pillar

Atsushi Sainoki \*, Hani S. Mitri

Department of Mining and Materials Engineering, McGill University, Montreal, Canada, H3S1R7

### ABSTRACT

This study focuses on the instability mechanism of an isolated pillar, caused by time-dependent skin degradation and strength heterogeneity. The time-dependent skin degradation is simulated with a non-linear rheological model capable of simulating tertiary creep. The inherent strength heterogeneity is realized with Weibull's distribution. The results obtained from the analysis show that pillar degradation is limited to the regions near the surface or the skin until two months after ore extraction, but afterwards degradation starts to extend deeper into the pillar, eventually leaving a highly stressed pillar core due to stress transfer from the failed rock regions. Rockburst potential indices show that the risk increases exponentially at the core as time goes by. It is then demonstrated that the progressive skin degradation cannot be simulated with the conventional strain-softening model assuming brittle failure. The parametric study with respect to the degree of heterogeneity reveals that heterogeneity is key to the occurrence of progressive skin degradation. Although the average UCS in the model with a high degree of heterogeneity is almost the same as that in the model with a low degree of heterogeneity, degradation of the rockmass extends deep into the pillar only when the pillar material is highly heterogeneous.

KEYWORDS: pillar stability; underground mine; skin degradation; rheological model; time-dependent failure

### 1. INTRODUCTION

A pillar is a rockmass that remains to increase the stability of underground openings. The stability of isolated pillars is crucial because the failure of pillars can lead to fatal accidents and might cause the collapse of rockmass in an extensive area (Cording et al., 2015). Furthermore, pillars can be the cause for rockburst in the case of deep hard rock mines because of the high strain energy stored within the pillar and characteristics of rockmass exhibiting extremely brittle behaviour. Hence, the stability of isolated pillars needs to be evaluated and assessed in an appropriate manner.

A number of studies have been undertaken to estimate the stability of pillars (Martin et al., 2000). In addition, various empirical equations have been proposed for the estimation of a factor of safety (FOS) (Potvin et al., 1989; Sjöberg, 1992; Van der Merwe, 2003). Notwithstanding the significant efforts, pillars with a high FOS occasionally fail and collapse, which would be attributed to unknown uncertainties.

As such uncertainties, the strength heterogeneity of rockmass and time-dependent degradation of a pillar skin would be considered. Indeed, the degradation of a pillar skin, which is represented by spalling, scaling, or strength decay, has been studied by many researchers (Cording et al., 2015; Napier et al., 2012). The schematic illustration of spalling that takes place in a deep hard rock mine is delineated in Figure 1. As can be seen in the figure, due to the

spalling, the side wall of the pillar is loosened and loses load-bearing capacity, consequently inducing additional loads to the core of the pillar. When the region undergoing strength degradation is sufficiently large, FOS of the pillar can decrease to a critical value due to the increase in stress acting in the pillar and the decrease in the cross section of an intact region. In previous studies, the typical simulation technique to simulate the degradation of a pillar side wall is to employ an exponential function to estimate the time-dependent strength decay of rockmass or to decrease rockmass strength in a loosened region under low confining stress near a pillar surface. Importantly, both of the simulation techniques are based on field observations or unverified assumptions

The present study focuses on the time-dependent skin degradation of an isolated pillar due to the occurrence of creep behaviour that eventually leads to the critical failure of rockmass whilst considering the strength heterogeneity with Weibull's distribution (Weibull, 1951). The mechanism and process of stress transfer from loosened near-surface regions to the intact area of the pillar are investigated with the non-linear rheological constitutive model with input parameters derived from laboratory experiments. The comparison of the rheological model with the classical Mohr-Coulomb model taking into account brittle failure (strain-softening) is made in order to emphasize the importance of considering the time-dependent degradation of a pillar skin.

\*Atsushi Sainoki – email : atsushi.sainoki@mail.mcgill.ca

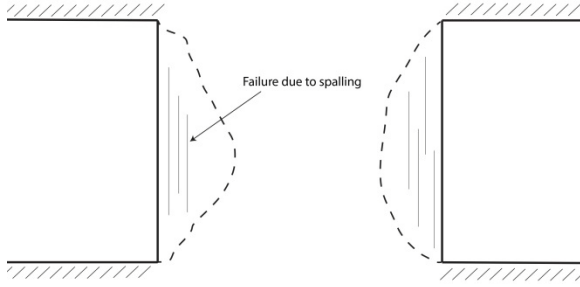


Figure 1: Schematic illustration of skin degradation of an isolated pillar due to spalling.

## 2. METHODOLOGY

### 2.1 Constitutive model

As indicated by Scholz (1968), the creep behaviour of rockmass is essentially the progressive development of microcracks, which pertains to the degradation of rockmass. Thus, the present study employs a creep model. To date, a number of constitutive models have been proposed and employed to simulate the creep behaviour of rockmass (Barla et al., 2012). Importantly, few of the models are capable of simulating tertiary creep that causes rockmass to fail. In order to take tertiary creep into consideration, the present study employs the non-linear rheological model proposed by Okubo et al. (2006). The advantage of the constitutive model over the other models considering tertiary creep (Barla et al. 2012) is that the analytical solution of creep lifetime, i.e., time to final rupture, is provided (Okubo et al., 2006).

The non-linear rheological model is expressed as follows:

$$\frac{d\lambda^*}{dt} = \frac{1}{t_0} \left( \frac{m}{n+1} \right)^{n-m+1} (\lambda^*)^m (\sigma^*)^n \quad (1)$$

where  $\lambda^*$  is compliance normalized by its initial value,  $\lambda_0$ ;  $\sigma^*$  is called severity;  $n$  and  $m$  represent the degree of time dependency and ductility of rock, respectively;  $t$  is time;  $t_0$  is time that it takes for the axial stress applied to a rock specimen to reach its peak axial value during an unconfined compression test. In the present study,  $t_0$  is determined whilst assuming a uniaxial test with a typical axial strain rate. The constants,  $n$  and  $m$ , for granite are taken from the database (Okubo et al., 2006). The constant,  $n$ , is derived from uniaxial compressive strengths obtained from unconfined compression tests under different axial strain rates, while the constant,  $m$ , is estimated from the shape of a post-peak behaviour curve (Okubo et al., 2006).

The severity,  $\sigma^*$ , is given using deviatoric stress as follows:

$$\sigma^* = \frac{\sigma_1 - \sigma_3}{\sigma_{\max} - \sigma_3} \quad (2)$$

where  $\sigma_1$  and  $\sigma_3$  are the maximum and minimum principal stresses, respectively;  $\sigma_{\max}$  is the maximum stress calculated from a failure criterion. Note that compression is a positive quantity in the equations. The severity for tensile failure is calculated as follows:

$$\sigma^* = \frac{|\sigma_3|}{\sigma_t} \quad (3)$$

where  $\sigma_t$  is the tensile strength of rock. The larger one of the severities determined by Equations (2) and (3) is adopted as  $\sigma^*$  and substituted into Equation (1). As Poisson's ratio,  $\nu$ , is expected to increase with the progression of rock degradation, Okubo et al. (1993) use the following equation to relate  $\nu$  with  $\lambda^*$ :

$$\nu = 0.5 - \frac{0.5 - \nu_0}{\lambda^*} \quad (4)$$

where  $\nu_0$  is an initial Poisson's ratio. The modulus of elasticity is calculated with  $\lambda^*$  as follows:

$$E = \frac{E_0}{\lambda^*} \quad (5)$$

where  $E_0$  is an initial value of modulus of elasticity. Regarding the failure criterion to calculate the severity, the classical Mohr-Coulomb failure criterion is employed because of its simplicity. As this study does not aim at calibrating analysis conditions and mechanical properties of rock based on actual field measurements, the use of the Mohr-Coulomb failure criterion is deemed sufficient. In addition to that, it is noteworthy that although Equations (1) to (5) indicate that compliance might increase even under initial stress conditions before mining activity starts, it has been confirmed that the increase in compliance is extremely small even when several hundred million years passed if there is no mining activity.

### 2.2 Generalized simulation procedure

When the non-linear rheological model is employed, an iterative analysis is carried out, of which the generalized procedure is shown in Figure 2. As can be seen in the figure, after the numerical model construction, in-situ stresses are applied if necessary. This means that when the time dependent behaviour of in-situ rockmass in an underground mine is examined, in-situ stress conditions need to be simulated. On the other hand, when the time-dependent behaviour of a rock specimen during a laboratory test is simulated, there is no need to apply such in-situ conditions to the model. As the present study applies the rheological model to two different numerical models representing a room-and-pillar mine and an unconfined compression test under a constant strain rate, the difference in the initial boundary conditions between the two numerical models is described for clarification. At the third step,

the conditions that cause creep behaviour are applied. In the case of room-and-pillar mining, the condition is ore extraction and the generation of an isolated pillar, while in the case of laboratory test, axial strain that increases with time, is applied to the top boundary of the rock specimen. Subsequently, a static analysis is carried out and if the elapsed time,  $t$ , has not yet reached the pre-determined  $t_{max}$ , the maximum and minimum stresses are computed for each zone. Then, the mechanical properties are updated according to Equations (1) to (5).

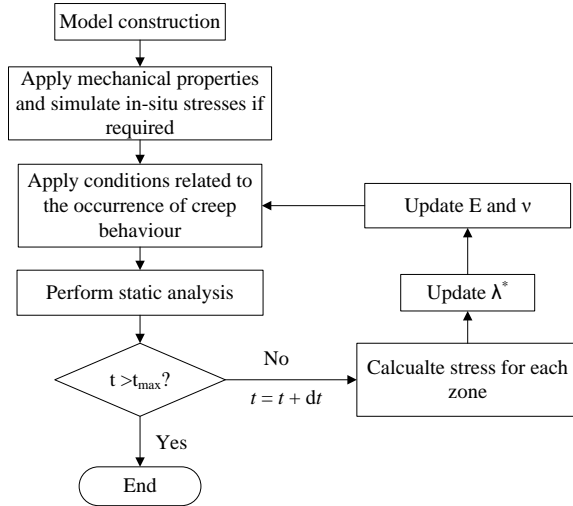


Figure 2: Procedure of iterative analysis.

### 2.3 Numerical model description

Figure 3 shows a 3D numerical model analyzed in the present study, which is constructed with FLAC3D (Itasca, 2009). The symmetry of the pillar is taken into account, that is, the pillar in the figure represents one-fourth of the actual pillar with the width of 10 m. The green-coloured region is extracted during analysis, and the dimension is determined so that the FOS of the pillar falls between 1.0 and 1.4. The FOS is evaluated with empirical equations (Potvin et al., 1989; Sjöberg, 1992). The stability of pillars with FOS in the range is uncertain (Martin, 2000) and assumed to be affected by a number of factors such as the time-dependent degradation. Thus, it is worth examining.

Pre-mining stress state is based on the equations proposed by Diederichs (1999). The mining depth is assumed to be 1500 m. The stresses computed from the equations are applied to each zone in the model. Note that the maximum horizontal stress is applied in the x-direction. Fixed boundary conditions are employed, that is, the displacements on the model outer boundaries are fixed in the direction perpendicular to the boundaries.

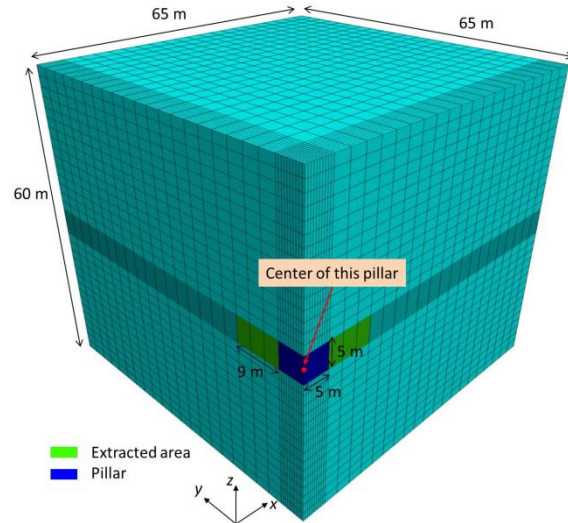


Figure 3: Numerical model analyzed.

### 2.4 Mechanical properties

Granite is assumed as the main type of rockmass composing the pillar. In order to convert mechanical properties obtained from laboratory experiments to those for the rockmass, RMR = 92 is assumed, which is the upper limit of rockmass encountered in the Canadian Shield (Martin, 2000). Herein, RMR is the rockmass rating system proposed by Bieniawski (1989). The mechanical properties of intact granite are derived from the study (Yun, 2008). Using the RMR, the deformation modulus,  $E$ , in Table 1 is obtained with the equation (Mitri et al., 1994). The uniaxial compressive strength is calculated with the Hoek-Brown failure criterion while substituting  $\sigma_3 = 0$ . The tensile strength is assumed to be one-tenth of the uniaxial compressive strength (Tesarik et al, 2003). For the constants in Equation (1),  $n = 51$  and  $m = 51$  are derived for granite (Okubo et al., 2006).

Table 1: Mechanical properties of granite for rockmass.

E (GPa)	v	$\sigma_c$ (MPa)	C (MPa)	$\phi$ (°)	$\sigma_T$ (MPa)	Density (kg/m <sup>3</sup> )
59	0.26	116	14.8	63	11.6	2600

### 2.5 Strength heterogeneity of rockmass

The inherent strength heterogeneity of rockmass is taken into account with the Weibull's distribution, which is expressed as:

$$f(u) = \frac{\alpha}{u_0} \left(\frac{u}{u_0}\right)^{\alpha-1} \exp\left[-\left(\frac{u}{u_0}\right)^\alpha\right] \quad (6)$$

where  $u$  and  $u_0$  are a mechanical property and a scale parameter related to the average value of the mechanical property, respectively;  $\alpha$  represents the degree of heterogeneity. In a base model,  $\alpha = 5$  is

taken. Figure 4 shows the heterogeneity of UCS for the case.

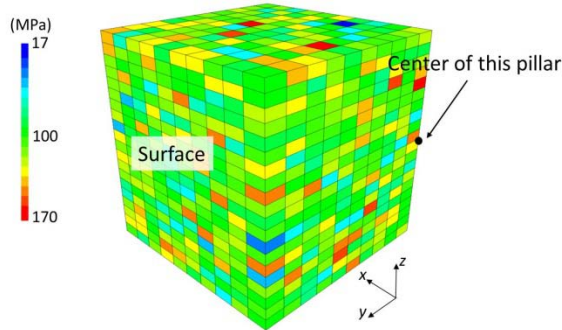


Figure 4: Heterogeneity of UCS simulated with the Weibull's distribution ( $\alpha = 5$ ).

### 2.5 Determination of upper limit of $\lambda^*$

Although the rheological model assumes that  $\lambda^*$  increases infinitely, its upper limit needs to be determined to ensure computational stability. To do so, a uniaxial test is simulated with a cylindrical model under a constant strain rate. When the upper limit is low, the strain softening during post-peak behaviour is not sufficiently simulated. During the simulation, displacements are applied to the top boundary at the third step in Figure 2. Analyses are performed while changing the upper limit from 50 to 1000. It is then found that when the upper limit is 1000, brittle behaviour is adequately replicated. It should be noted, however, that when the brittle failure takes place,  $\lambda^*$  does not reach 1000 in all the zones because failure takes place locally. Thus, it is not appropriate to apply the upper limit to the pillar model, directly. In light of the result, the average value of  $\lambda^*$  in the cylindrical model at the failure is computed. The computed average is near 285. Thus, after rounding up, the upper limit is set to 300 for the pillar model.

## 3. RESULTS

### 3.1 Time-dependent skin degradation

Figure 5 shows change in the maximum compressive stress within the pillar with time. It is found from the figure that the pillar surface can carry stress immediately after the extraction. The low stress regions are limited to the zones with particularly low initial strength. There is no noticeable change in the stress state until 33 days after the extraction. However, when 72 days have passed, low stress regions extend to almost entire the surface, indicating that the rockmass near the surface lost load-bearing capacity due to the time-dependent degradation. After 187 days, the degradation of rockmass extends deeper into the pillar, and the pillar core carries extremely high stresses due to the stress transfer from

the failed regions. This indicates that the pillar becomes extremely burst-prone.

In order to investigate the burst proneness of the pillar, brittle shear ratio (BSR) proposed by Castro et al. (2012) and burst prone index (BPI) proposed by Mitri (1999) are computed at the center of the pillar. As can be seen from Figure 6, both of the indices do not show a noticeable increase until 72 days, whereas, after that, the indices increase exponentially, indicating that the failure propagation becomes uncontrolled. Eventually, after 226 days have passed, BPI and BSR increase to 222% and 1.33, respectively. As expected, both the values indicate extremely high possibility of a rockburst taking place.

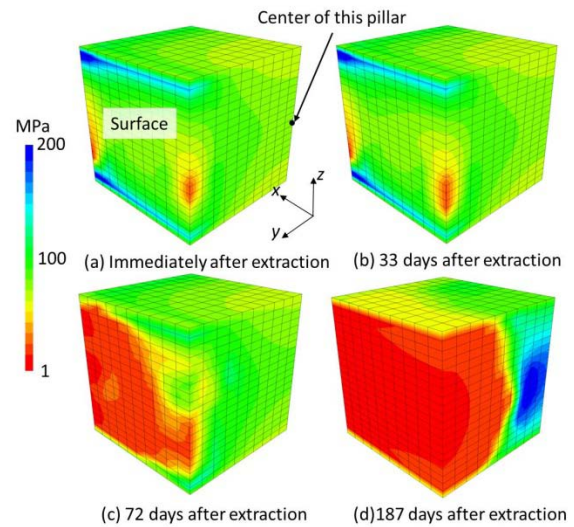


Figure 5: Maximum compressive stress in the pillar.

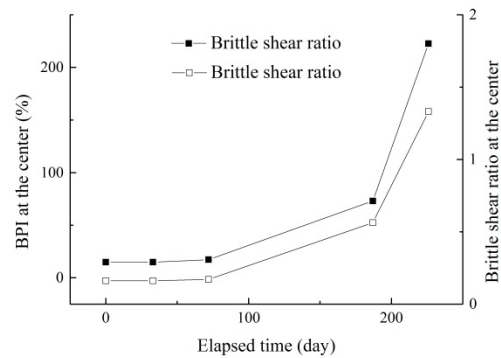


Figure 6: Burst proneness at the center of the pillar.

### 3.2 Comparison with strain-softening model

In order to make the difference between the non-linear rheological model and the conventional strain-softening model clearer, the comparison between the models is made. The strain-softening model employs the conventional Mohr-Coulomb criterion with the

consideration to strain-softening behaviour, that is, when failure takes place, the cohesion is decreased to zero. A static analysis is conducted with the same model as shown in Figure 4.

Figure 7 shows the maximum compressive stress obtained from the analysis. Remarkably, there is a clear difference in the stress state within the pillar between the models. When the strain-softening model is employed, the region with low stresses occurs only near the surface. The considerably high stresses at the pillar core shown in Figure 5(d) are not found in Figure 7, implying that the use of the conventional model might underestimate the possibility of failure when there is the heterogeneity of strength. Conversely, when the rockmass is completely homogeneous, there will be no large difference between the two models.

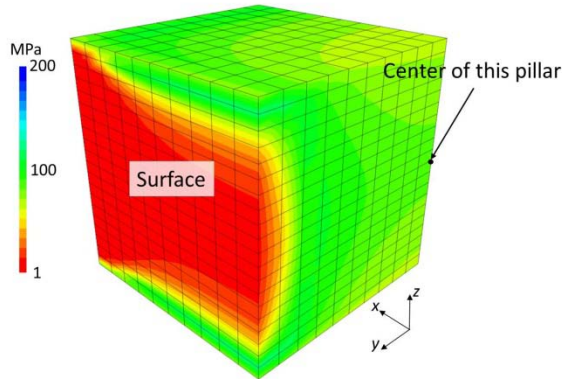


Figure 7: Maximum compressive stress obtained from strain-softening model.

### 3.3 Effect of degree of strength heterogeneity

In addition to the model shown in Figure 4, another model is constructed with  $\alpha = 6$  in Equation (6). The model is shown in Figure 8. The larger  $\alpha$ , the more homogeneous the model becomes. Except for the parameter, the same procedure is taken. Interestingly, the analysis reveals that the progressive skin degradation does not occur even after 7 years when  $\alpha = 6$ . It should be noted that, in terms of an average UCS in the pillar, there is no large difference between the two models. Indeed, the average UCS is 107 MPa and 108 MPa for the models with  $\alpha = 5$  and 6, respectively. It is thus unlikely that the occurrence of the intensive degradation of rockmass shown in Figure 5 is determined by the slight difference in the average UCS.

In light of the results and with respect to each zone in the pillar, the minimum UCS in adjacent zones is investigated. Figure 8 shows the results. For instance, when  $\alpha = 5$ , the number of zones that have adjacent zones with UCS between 30 MPa and 50 MPa is approximately 240. The figure obviously displays the difference between the two models.

When  $\alpha$  is low, the possibility that zones with low UCS are present in the vicinity of each zone is clearly higher. From the figure, it can be deduced that the intensive skin degradation shown in Figure 5(d) occurs due to the chain effect of failure through zones with low UCS, i.e., stress transferred from a failed zone causes failure in adjacent zones, which eventually escalates into the chain effect. Zones with extremely low UCS exist even when  $\alpha = 6$ . However, in order for the failure to propagate to adjacent zones, zones with low UCS must exist in the vicinity of the failed zone. When  $\alpha = 5$ , it is assumed that the conditions are satisfied, so that the failure becomes uncontrolled after sufficient time has elapsed. Importantly, the chain effect cannot be adequately simulated with the strain-softening model as shown in Figure 7 because the non-linear rheological model simulates strength degradation with tertiary creep even if the maximum stress is less than the maximum strength.

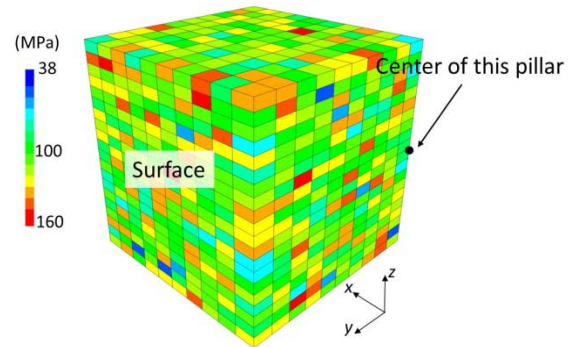


Figure 8: Heterogeneity of UCS simulated with the Weibull's distribution ( $\alpha = 6$ ).

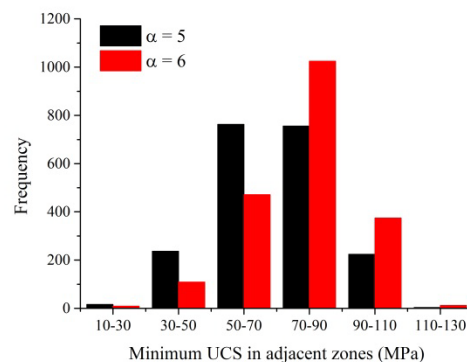


Figure 9: Relation between minimum UCS of adjacent zones and the total number of zones with the adjacent zones within the pillar.

## 4. CONCLUSIONS

The time-dependent skin degradation of an isolated pillar in a deep hard rock mine is simulated with a non-linear rheological model whilst taking into

account the inherent strength heterogeneity of the rockmass. Analysis results show that the skin degradation extends deep into the pillar when sufficient time has elapsed, resulting in a highly stressed pillar core due to the stress transfer from the failed region. Rockburst potential indices calculated at the core show extremely high risk for rockburst. The analysis conducted with the conventional strain-softening model demonstrates that the propagation of skin degradation into the inside of the pillar cannot be replicated with the strain-softening model, emphasizing the importance of the time-dependent skin degradation. The propagation of failure into the inside of the pillar is not simulated in the model with lesser strength heterogeneity, although an average UCS within the pillar is almost the same for the two models. It is then deduced that the presence of adjacent zones with low UCS is a key to the progressive skin failure because it gives rise to the chain effect of failure with stress transfer from the failed zone to the adjacent zones.

## 5. ACKNOWLEDGEMENT

This work is financially supported by a grant by the Natural Science and Engineering Research Council of Canada (NSERC) in partnership with Vale Ltd – Sudbury Operations, Canada, under the Collaborative Research and Development Program. The authors are grateful for their support.

## 6. REFERENCES

Barla, G., Debernardi, D., & Sterpi, D. (2012). Time-dependent modeling of tunnels in squeezing conditions. *International Journal of Geomechanics*, Volume 12(6), pp. 697-710

Bieniawski, Z. T. (1989). *Engineering rock mass classifications*. Wiley, New York

Castro, L.A.M., Bewick, R.P., & Carter, T.G. (2012). An overview of numerical modelling applied to deep mining. *Innovative Numerical Modelling in Geomechanics*, pp. 393-414.

Cording, E.J., Hashash, Y.M.A., & Oh, J. (2015). Analysis of pillar stability of mined gas storage caverns in shale formations. *Engineering Geology*, Volume 184, pp. 71-80

Diederichs, M.S. (1999). *Instability of hard rockmass: the role of tensile damage and relaxation* (PhD), University of Waterloo, Waterloo, Canada.

Itasca. (2009). *FLAC3D - fast Lagrangian analysis of continua* (Version 4.0). U.S.A.: Itasca Consulting Group Inc. .

Martin, C.C., & Maybee, W.G. (2000). The strength of hard-rock pillars. *International Journal of Rock Mechanics and Mining Science*, 37, 1239-1246.

Mitri, H.S., Edrissi, R., & Henning, J. (1994). Finite element modelling of cable-bolted stopes in hardrock ground mines. Paper presented at the SME Annual Meeting, Albuquerque, New Mexico.

Mitri, H.S., Tang, B., & Simon, R. (1999). FE modelling of mining-induced energy release and storage rates. *Journal South African Institute of Mining and Metallurgy*, 99(2), 103-110.

Napier, J.A.L., & Malan, D.F. (2012). Simulation of time-dependent crush pillar behaviour in tabular platinum mines. *The Journal of The South African Institute of Mining and Metallurgy*, 112, 711-719.

Okubo, S., & Fukui, K. (2006). An analytical investigation of a variable-compliance-type constitutive equation. *Rock Mech. Rock Eng.*, 39(3), 233-253.

Okubo, S., & Jin, F. (1993). Simulation of rock behaviour around circular roadway by non-linear rheological model. *Journal of the Mining and Materials Processing Institution of Japan*, 109, 209-214.

Potvin, Y., Hudyma, M.R., & Miller, H.D.S. (1989). Design guidelines for open stope support. Paper presented at the Bull Can Min Metall.

Scholz, C.H. (1968). Mechanism of creep in brittle rock. *Journal of Geophysical Research*, 73(10), 3295-3302.

Sjöberg, J. (1992). Failure modes and pillar behaviour in the Zinkgruvan mine. Paper presented at the 33rd U.S. Rock Mechanics Symposium, Sante Fe. Rotterdam.

Tesarik, D.R., Seymour, J.B., & Yanske, T.R. (2003). Post-failure behaviour of two mine pillars confined with backfill. *International Journal of Rock Mechanics and Mining Science*, 40(2), 221.

Van der Merwe, J.N. (2003). New pillar strength formula for South African Coal. *The Journal of The South African Institute of Mining and Metallurgy*, 103(5), 281-292.

Weibull, W.A. (1951). Statistical distribution function of wide applicability. *Journal of applied mechanics*, 18, 293-297.

Yun, Xiaoyou. (2008). *Geomechanical behaviour of biaxially loaded rock*. (PhD), McGill University, Montreal, Canada.